Magnetic Resonance Spectroscopy and Imaging Can Differentiate Between Engineered Bone and Engineered Cartilage

Padmabharathi Pothirajan, Sriram Ravindran, Anne George, Richard L. Magin and Mrignayani Kotecha*

Abstract—**In the situation when both cartilage and its underlying bone are damaged, osteochondral tissue engineering is being developed to provide a solution. In such cases, the ability to non-invasively monitor and differentiate the development of both cartilage and bone tissues is important. Nuclear magnetic resonance (NMR) spectroscopy and magnetic resonance imaging (MRI) have been widely used to non-invasively assess tissue-engineered cartilage and tissue-engineered bone. The purpose of this work is to assess differences in MR properties of tissue-engineered bone and tissue-engineered cartilage generated from the same cell-plus-scaffold combination at the early stage of tissue growth. We developed cartilage and bone tissue constructs by seeding human marrow stromal cells (HMSCs, 2 million/ml) in 1:1 collagen/chitosan gel for four weeks. The chondrogenic or osteogenic differentiation of cells was directed with the aid of a culture medium containing chondrogenic or osteogenic growth factors, respectively. The proton and sodium NMR and water-proton T_1, T_2 and diffusion MRI experiments were performed on these constructs and the control collagen/chitosan gel using a 9.4 T (^{1}H freq. = 400 MHz) and a 11.7 T (^{1}H freq. = 500 MHz) NMR spectrometers. In all cases, the development of bone and cartilage was found to be clearly distinguishable using NMR and MRI. We conclude that MRS and MRI are powerful tools to assess growing osteochondral tissue regeneration.**

I. Introduction

Musculoskeletal disorders are a major cause of disability and discomfort among adults in the United States [4]. Osteoarthritis, trauma, developmental issues, sports injuries, and motor accidents commonly cause damage to cartilage and, in many cases, its underlying subchondral bone. Currently, there are few treatment options available to treat an osteochondral defect. These include microfracture, osteochondral autografts and allographs transplantation, and autologous chondrocyte implantation (ACI), however, none of these treatment provide a long-term cure for osteochondral defects [5-7]. Osteochondral tissue engineering is expected to provide solutions by offering a tissue with biochemical and mechanical properties of cartilage on one end, bone on the other end and a smooth osteochondral interface in between [8, 9]. This requires complex tissue-engineering approaches and advanced assessment techniques. Cartilage is comprised of tissue-water, proteoglycans, collagen type II and chondrocytes arranged in a zonal environment. Each component of cartilage plays a specific role in its mechanical properties. The subchondral bone is made of water, collagen type I, and hydroxyapatite crystals. The compressive strength of bone is much higher (~6 GPa) when compared to the cartilage (~ 0.8, 2, and 320 MPa in superficial, middle and deep cartilage zones) [9]. These differences in the biomechanical properties of cartilage and bone are a challenge for osteochondral tissue engineering.

Development of non-invasive assessment techniques goes hand-in-hand with the development of tissue engineering approaches. Magnetic resonance spectroscopy and imaging are the leading non-invasive characterization tools for engineered cartilage and bone tissues [10-17]. Much of the current efforts in MR characterization are focused on tissue-engineered cartilage, however at the osteochondral interfaces, the comparative MR properties of cartilage and bone tissues during the growth phase are of utmost interest. In this study, for the first time, we tabulate differences in the MR properties of tissue-engineered osteogenic and chondrogenic constructs developed using same a cells-plus-scaffold combination. We performed water-suppressed proton NMR spectroscopy, proton and sodium relaxation time (T_1, T_2) measurements, sodium triple-quantum coherence NMR spectroscopy, and water-proton diffusion MRI.

II. Materials and Methods

A. Bone and Cartilage Tissue Construct Preparation

Figure 1 shows the schematic of sample preparation. Briefly, human marrow stromal cells (HMSCs, 2 million/ml) were seeded in in a 1:1 co-polymer matrix comprising of 1mg/ml type I collagen and 1 mg/mL chitosan as explained previously [11]. The osteogenic differentiation of HMSCs was directed with the aid of 100 μg/mL ascorbic acid, 10 mM β-glycerophosphate, and 10 mM dexamethasone in the differentiation media, whereas the chondrogenic differentiation was directed with the aid of 1% FBS, 1 mM

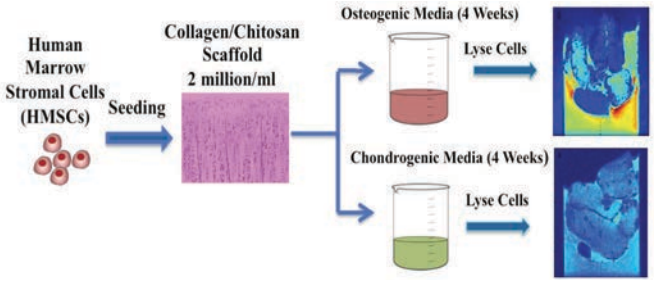

Figure 1: The schematic of chondrogenic and osteogenic construct preparation. The last column shows T_2 weighted MRI images.

Research partially supported by NIH/NIBIB grant EB 007537 and NIH/NIDCR grant DE11657.

M. Kotecha is with the Department of Bioengineering, University of Illinois at Chicago, Chicago, IL 60612 USA (phone: 312-413-2018; fax: 312-996-5921; e-mail: mkotecha@uic.edu).

P. Pothirajan and R. Magin are with the Department of Bioengineering, University of Illinois at Chicago, Chicago, IL 60612 USA (e-mails: ppothi2@uic.edu, rmagin@uic.edu).

S. Ravindran and A. George are with the Department of Oral Biology, University of Illinois at Chicago, Chicago, IL 60612 USA (e-mails: sravin1@uic.edu>, anneg@uic.edu).

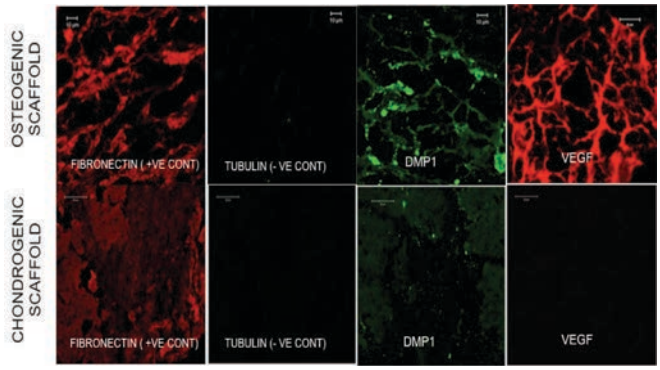

Figure 2: Representative confocal images of osteogenic and chondrogenic scaffolds stained for different ECM proteins. Fibronectin was used as positive control and tubulin served as negative control for the presence of intracellular protein. It is evident from the image that osteogenic proteins such as DMP1 were present in negligible quantities in the chondrogenic scaffold. DMP1 protein in small quality has been found to be essential for cartilage growth as evident from these references [2, 3]. Additionally, VEGF, the pro angiogenic growth factor was absent in the chondrogenic scaffold. Cartilage being an avascular tissue necessitates that the chondrogenic scaffolds should not promote vascularization *in vivo.* Therefore, the absence of VEGF and reduced DMP1 indicated that the chondrogenic scaffold was anti osteogenic and pro chondrogenic in nature.

dexamethasone, 50 mg/mL ascorbate-2 phosphate and 10 ng/ml TGF-β in αMEM differentiation media. The samples were decellularized as explained in our recent article [11] and kept at 4 °C prior to MR experiments. Biochemical analysis at the end of four week confirmed osteogenic and chondrogenic extracellular matrix preparation as shown in Figure 2.

B. Proton NMR Experiments

The NMR experiments were performed at 298 K using a 9.4 T (^{1}H freq. = 400.132 MHz) or a 11.7 T (500 MHz) Bruker Avance spectrometer equipped with a broadband probe. Samples were placed in 99% D_2O.

(a) Water suppressed proton NMR: The water suppression was achieved using the excitation sculpting Bruker "zgesgp" sequence [18]. The experimental parameters were as follows: proton 90° pulse width = 11 μs, relaxation delay = 1 s, number of points in FID = 8192, number of scans = 16, spectral window = 15 kHz, soft 180° pulse shape = square, duration of soft pulse = 2 ms, gradient shape = sin, gradient duration = 1 ms. The free induction decay (FIDs) were processed by using a 4 Hz exponential window function and zero order phase correction. The Bernstein polynomial fit was used for baseline correction.

(b) Proton relaxation time (T_1, T_2) measurements: The 90° pulse width was 14 μs and relaxation delay was 3 s. The other experimental parameters were: no. of scans = 16, no. of points in FID = 16k, sw = 12 kHz. The T_1 experiments were performed using the inversion-recovery pulse sequence 180°- τ - 90°- acq with delay τ (16 steps) = 1 ms, 5 ms, 7.5 ms, 10 ms, 20 ms, 35 ms, 50 ms, 75 ms, 100 ms, 200 ms, 500 ms, 750 ms, 1 s, 2 s, 5 s and 10 s. The T_2 experiments were performed using the standard Carr-Purcell-Meiboom-Gill (CPMG) pulse sequence using the echo time 7 ms and number of steps: 2, 4, 8, 10, 12, 16, 20, 24, 32, 48, 64, 84, 96, 128, 200 and 256. The relaxation values were calculated by fitting the signal intensity to the single exponential curves, $M_{xy}(t) = M_{xy0}*e(-t/T_2)$ and $M_z(t) = M_{z0}*\{1-2*e(-t/T_1)\}$.

C. Sodium NMR Experiments

The sodium NMR experiments were performed using a 9.4 T (^{23}Na freq. 105.83 MHz) using a broadband probe. Samples were placed in phosphate buffer saline (PBS). The 90° pulse width and relaxation delay were 9.15 μs and 100 ms for all sodium NMR experiments. The other experimental parameters were = no. of scans = 16, no. of points in FID = 1024, sw = 10 kHz. The T_1 experiments were performed using the inversion recovery pulse sequence 180°- τ - 90°-acq with delay τ (16 steps) = 0.5, 1, 2, 5, 7.5, 10, 20, 50, 75, 80, 100, 200, 500, 750, 800 and 1000 ms. The T_2 experiments were performed using the standard Carr-Purcell-Meiboom-Gill (CPMG) pulse sequence using the echo time 1 ms and number of steps: 2, 4, 8, 10, 12, 16, 32, 48, 64, 128, 176 and 256. The relaxation values were calculated by fitting the signal intensity to the single exponential curve as explained in the proton NMR experiment details.

The sodium triple-quantum coherence signal spectra were acquired using the standard four-pulse triple-quantum coherence filter sequence $90°_{\Phi1}$- τ/2-$180°_{\Phi2}$- τ/2-$90°_{\Phi3}$-δ-$90°_{\Phi4}$, with $\Phi_1 = \Phi_2 = \Phi$; $\Phi_3 = \Phi + \pi/2$, $\Phi_4 = 0$, where Φ was cycled through 30°, 90°, 150°, 210°, 270° and 330° to select the triple-quantum coherence [19, 20]. The other experimental parameters were: no. of scans =432, no. of points in FID = 1024, sw = 10 kHz. The preparation delay τ was varied as 0.5, 1, 2, 5, 8, 10, 15, 20, 25, 30, and 40 ms. The fast (T_f) and the slow (T_s) relaxation times were calculated using a custom written Matlab program based on the method described in our published article [20].

D. MRI Experiments

The MRI measurements were performed using a Bruker 500 MHz (11.7 T) micro-imaging facility controlled by the Bruker imaging software Paravision 4.0. The samples were washed using Hank's balanced salt solution (HBSS) and placed on top of a 1% agarose gel in a 5 mm tube. Flourinert oil was added for filling the rf coil volume. The T_2 weighted images were acquired using the FLASH sequence with TE/TR = 13/1000 ms, FOV = 6 mm x 6 mm, matrix size = 128 x 128, and slice thickness = 0.5 mm was chosen. The apparent diffusion coefficient (ADC) was obtained using a diffusion weighted spin echo MRI sequence. The experimental parameters were TE = 25.6 ms, TR = 5000ms, b-values (s/mm^2) = 13, 213, 513, 813, 1213, 1613. The ADC maps were calculated by fitting voxel-by-voxel signal intensity to the single exponential fitting curve using a custom written Matlab program. The average ADC was derived from the ROI of the sample area.

III. Results and Discussion

A. Water-Suppressed Proton NMR Spectra

Figure 3 shows the water-suppressed proton NMR spectra of the control chitosan/collagen gel, osteogenic and chondrogenic constructs in 99% D_2O. The water peak was used as an internal chemical shift reference in these spectra. The dominating resonances can be assigned to metabolites

related to the observed tissue or chitosan/collagen based on the literature [21-26]. A few important points can be noted from the figure: (a) resonances in osteogenic constructs are sharper when compared to the chondrogenic constructs. Since the spectra were acquired in D_2O, this might be due to the presence of fast proton exchange in these samples, (b) the resonance in chondrogenic constructs at 2 ppm (typically assigned to the N-acetyl peak in cartilage) appear to be broad in these samples when compared to published literature on cartilage [27].

B. Proton relaxation times

The water-proton relaxation times are given in Table 1. It is interesting to note that the T_2/T_1 ratio is smaller in osteogenic constructs when compared to the chondrogenic constructs. According to the Bloembergen-Purcell-Pound (BPP) theory [1] of water relaxation, the ratio T_2/T_1 is an indication of the water environment as shown in Figure 4. The smaller ratio for osteogenic tissues is a sign of complex or more solid osteogenic constructs when compared to the chondrogenic constructs.

C. Sodium relaxation times

Table 2 gives values of sodium relaxation times. Interestingly, the sodium T_2/T_1 ratio is also smaller in osteogenic samples when compared to chondrogenic samples. Interestingly, the ratio T_2/T_1 is close to 1 in chondrogenic samples. Sodium is a spin 3/2 nucleus and its relaxation is dominated by quadrupolar coupling, therefore it is possible to get information about intra-molecular mobility and orientation information from sodium NMR. Since the T_2/T_1 ratio is close to 1 in chondrogenic samples, it is possible that they possess an isotropic-like environment that makes the average quadrupolar coupling in these samples close to zero [20]. This is further confirmed by sodium triple-quantum coherence spectroscopy on these constructs.

In our recent publication, we used sodium triple-quantum (TQ) coherence spectroscopy to assess tissue-engineered cartilage in the presence of cells and growth culture media [20]. In the current study, we used sodium TQ spectroscopy

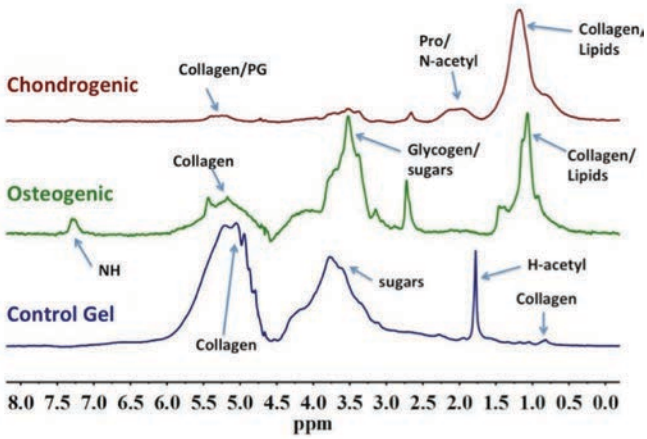

Figure 3: Water-suppressed proton NMR spectra of control collagen/chitosan gel, osteogenic, and chondrogenic constructs.

Table 1: Proton relaxation times at 11.7 T.

Tissue Samples	T_1 (s)	T_2 (ms)	T_2/T_1
Osteogenic (n= 4)	5.2 (± 0.1)	1347 (± 56)	0.26
Chondrogenic (n= 4)	5.1 (± 0.1)	1612 (± 105)	0.31
Collagen/Chitosan Gel	5.0 (± 0.02)	2935 (± 52)	0.59

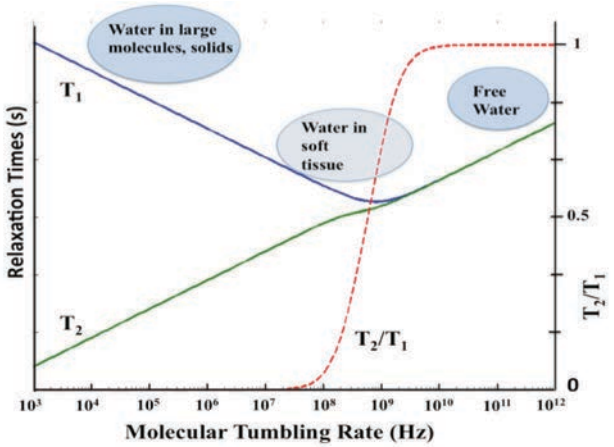

Figure 4: Water T_1, T_2, and the ratio T_2/T_1 at 500 MHz resonance frequency as a function of the molecular tumbling rate according to BPP theory [1].

Table 2: Sodium relaxation times at 11.7 T.

Tissue Samples	Sodium relaxation times			Sodium TQ coherence spectroscopy	
	T_1(ms)	T_2 (ms)	T_2/T_1	T_f(ms)	T_s (ms)
Osteogenic (n= 4)	43.3 (± 0.3)	29.4 (± 1.5)	0.68	48.3 (± 5)	4.6 (±0.5)
Chondrogenic (n= 4)	49.7 (± 0.4)	47.2 (± 1.1)	0.95	No TQ build up	
Collagen/Chitosan Gel	52.2 (± 0.1)	39.0 (± 0.3)	0.75	64 (±11)	19.5 (± 3)

to assess decellularized bone and cartilage engineered constructs. Surprisingly, we found that there was no sodium TQ build-up in chondrogenic scaffolds in the absence of cells. This leads us to the assumption that the sodium ions in these tissues are in an isotropic-like environment. It is possible that the random-collagen environment is responsible for the absence of anisotropy in these tissues. We found that the sodium TQ signal was strong for osteogenic scaffolds and weaker, but still positive in the collagen/chitosan gel. This shows that the gel and osteogenic constructs have an anisotropic tissue environment leading to a non-zero average quadrupolar coupling in these constructs. It would be interesting to investigate in future whether the initiation of vascularization is responsible for anisotropy in osteogenic constructs.

D. Diffusion MRI

The water diffusion coefficient is an established parameter for assessing tissue microstructure [28]. Figure 5 shows the apparent diffusion coefficient (ADC) maps for the control collagen/chitosan gel, osteogenic and chondrogenic constructs. It was found that the ADC values are higher for osteogenic constructs when compared to the chondrogenic

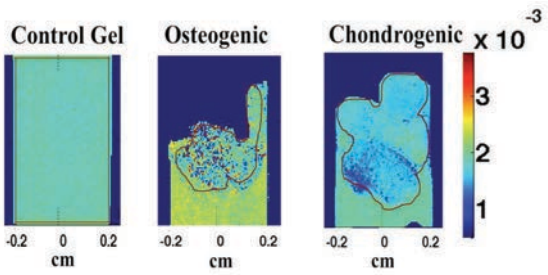

	Control Gel	Osteogenic (n = 4)	Chondrogenic (n =4)
ADC (mm^2/s)	1.87 (± 0.1) x 10^{-3}	1.97 (± 0.8) x 10^{-3}	1.6 (± 0.2) x 10^{-3}

Figure 5: ADC maps and calculated ADC values for control gel, osteogenic and chondrogenic constructs.

constructs. It is interesting to note the mixture of very low and high ADC values in osteogenic constructs whereas chondrogenic constructs are more homogeneous. It is possible that mineral deposits in osteogenic constructs are responsible for these low ADC spots.

IV. Conclusions

This study demonstrates that NMR and MRI are sensitive tools to differentiate between engineered chondrogenic and osteogenic tissues. That both osteogenic and chondrogenic constructs had clearly distinguishable MR properties at the early stage of growth is very positive and encouraging for future *in vivo* studies. We demonstrated that NMR and MRI could be used to characterize, assess and monitor growth at osteochondral interfaces.

References

[1] N. Bloembergen, E.M. Purcell, and R.V. Pound: "Relaxation Effects in Nuclear Magnetic Resonance Absorption", Physical Review, 1948, 73, (7), pp. 679-712.

[2] Y. Sun, S. Ma, J. Zhou, A.K. Yamoah, J.Q. Feng, R.J. Hinton, and C. Qin: "Distribution of Small Integrin-binding Ligand, N-linked Glycoproteins (SIBLING) in the Articular Cartilage of the Rat Femoral Head", Journal of Histochemistry & Cytochemistry, 2010, 58, (11), pp. 1033-1043.

[3] L. Ye, Y. Mishina, D. Chen, H. Huang, S.L. Dallas, M.R. Dallas, P. Sivakumar, T. Kunieda, T.W. Tsutsui, A. Boskey, L.F. Bonewald, and J.Q. Feng: "Dmp1-deficient mice display severe defects in cartilage formation responsible for a chondrodysplasia-like phenotype", J Biol Chem, 2005, 280, (7), pp. 6197-6203.

[4] "Prevalence and most common causes of disability among adults--United States, 2005", MMWR Morb Mortal Wkly Rep, 2009, 58, (16), pp. 421-426.

[5] A.J. Detterline, S. Goldberg, B.R. Bach, Jr., and B.J. Cole: "Treatment options for articular cartilage defects of the knee", Orthop Nurs, 2005, 24, (5), pp. 361-366; quiz 367-368.

[6] M. Zengerink, P.A. Struijs, J.L. Tol, and C.N. van Dijk: "Treatment of osteochondral lesions of the talus: a systematic review", Knee surgery, sports traumatology, arthroscopy : official journal of the ESSKA, 2010, 18, (2), pp. 238-246.

[7] C.P. Hannon, N. Baksh, H. Newman, C.D. Murawski, N.A. Smyth, and J.G. Kennedy: "A systematic review on the reporting of outcome data in studies on autologous osteochondral transplantation for the treatment of osteochondral lesions of the talus", Foot & ankle specialist, 2013, 6, (3), pp. 226-231.

[8] S.P. Nukavarapu, and D.L. Dorcemus: "Osteochondral tissue engineering: current strategies and challenges", Biotechnology advances, 2013, 31, (5), pp. 706-721.

[9] P. Nooeaid, V. Salih, J.P. Beier, and A.R. Boccaccini: "Osteochondral tissue engineering: scaffolds, stem cells and applications", J Cell Mol Med, 2012, 16, (10), pp. 2247-2270.

[10] M. Kotecha, D. Klatt, and R.L. Magin: "Monitoring cartilage tissue engineering using magnetic resonance spectroscopy, imaging, and elastography", Tissue Engineering Part B, 2013, 19, (6), pp. 470-484.

[11] S. Ravindran, Q. Gao, M. Kotecha, R.L. Magin, S. Karol, A. Bedran-Russo, and A. George: "Biomimetic Extracellular Matrix-Incorporated Scaffold Induces Osteogenic Gene Expression in Human Marrow Stromal Cells", Tissue Eng Pt A, 2012, 18, (3-4), pp. 295-309.

[12] S. Ramaswamy, J.B. Greco, M.C. Uluer, Z.J. Zhang, Z.L. Zhang, K.W. Fishbein, and R.G. Spencer: "Magnetic Resonance Imaging of Chondrocytes Labeled with Superparamagnetic Iron Oxide Nanoparticles in Tissue-Engineered Cartilage", Tissue Eng Pt A, 2009, 15, (12), pp. 3899-3910.

[13] P. Pothirajan, S. Ravindran, and M. Kotecha: 'Differences in Magnetic Resonance Properties of Osteogenic and Chondrogenic ECM scaffolds'. Proc. BMES-midwest career fair, Chicago, April 19th 2013.

[14] P. Pothirajan, S. Ravindran, and M. Kotecha: 'Magnetic Resonance Characterization of ECM-integrated scaffolds for bone and cartilage tissue engineering'. Proc. Annual meeting of Biomedical Engineering Society (BMES), Seattle, WA, Sept 25-28 2013.

[15] I.A. Peptan, L. Hong, H.H. Xu, and R.L. Magin: "MR assessment of osteogenic differentiation in tissue-engineered constructs", Advances in experimental medicine and biology, 2006, 12, (4), pp. 843-851.

[16] M. Kotecha, T.M. Schmid, B. Odintsov, and R. Magin: 'Reduction of water diffusion coefficient with increased engineered cartilage matrix growth observed using MRI'. IEEE-EMB, Chicago, Aug 26-30 2014.

[17] P. Pothirajan, D.L. Dorcemus, S. Nukavarapu, and M. Kotecha: 'True MRI assessment of stem cell chondrogenesis in a tissue engineered matrix'. IEEE-EMB, Chicago, Aug 26 - 30 2014.

[18] T.L. Hwang, and A.J. Shaka: "Water Suppression That Works. Excitation Sculpting Using Arbitrary Wave-Forms and Pulsed-Field Gradients", J Magn Reson, Series A, 1995, 112, (2), pp. 275-279.

[19] A. Borthakur, E. Mellon, S. Niyogi, W. Witschey, J.B. Kneeland, and R. Reddy: "Sodium and T-1 rho MRI for molecular and diagnostic imaging of articular cartilage", Nmr Biomed, 2006, 19, (7), pp. 781-821.

[20] M. Kotecha, S. Ravindran, T.M. Schmid, A. Vaidyanathan, A. George, and R.L. Magin: "Application of sodium triple-quantum coherence NMR spectroscopy for the study of growth dynamics in cartilage tissue engineering", NMR in biomedicine, 2013, 26, (6), pp. 709-717.

[21] W. Ling, R.R. Regatte, M.E. Schweitzer, and A. Jerschow: "Characterization of bovine patellar cartilage by NMR", NMR in biomedicine, 2008, 21, (3), pp. 289-295.

[22] J. Schiller, D. Huster, B. Fuchs, L. Naji, J. Kaufmann, and K. Arnold: "Evaluation of cartilage composition and degradation by high-resolution magic-angle spinning nuclear magnetic resonance", Methods in molecular medicine, 2004, 101, pp. 267-285.

[23] T. Riemer, A. Nimptsch, K. Nimptsch, and J. Schiller: "Determination of the glycosaminoglycan and collagen contents in tissue samples by high-resolution 1H NMR spectroscopy after DCl-induced hydrolysis", Biomacromolecules, 2012, 13, (7), pp. 2110-2117.

[24] Q. Zhang, J.Z. Hu, D.N. Rommereim, M.K. Murphy, R.P. Phipps, D.L. Huso, and J.F. Dicello: "Application of high-resolution 1H MAS NMR spectroscopy to the analysis of intact bones from mice exposed to gamma radiation", Radiation research, 2009, 172, (5), pp. 607-616.

[25] ASTM Standard: 'F2260-03 Standard Test Method for Determining Degree of Deacetylation in Chitosan Salts by Proton Nuclear Magnetic Resonance (1H NMR) Spectroscopy', 'Book F2260-03 Standard Test Method for Determining Degree of Deacetylation in Chitosan Salts by Proton Nuclear Magnetic Resonance (1H NMR) Spectroscopy' (2012, edn.).

[26] S. Garrod, E. Humpfer, M. Spraul, S.C. Connor, S. Polley, J. Connelly, J.C. Lindon, J.K. Nicholson, and E. Holmes: "High-resolution magic angle spinning 1H NMR spectroscopic studies on intact rat renal cortex and medulla", Magnetic Resonance in Medicine, 1999, 41, (6), pp. 1108-1118.

[27] W. Ling, R.R. Regatte, M.E. Schweitzer, and A. Jerschow: "Characterization of bovine patellar cartilage by NMR", NMR in biomedicine, 2008, 21, (3), pp. 289-295.

[28] D. Le Bihan: "Looking into the functional architecture of the brain with diffusion MRI", Nat Rev Neurosci, 2003, 4, (6), pp. 469-480.